First-principles study of the layering at the free liquid Sn surface

L. Calderín,[1] L. E. González,[2] and D. J. González[2]
[1]*Department of Physics, Queen's University, Kingston, Ontario, Canada K7L 3N6*
[2]*Departamento de Física Teórica, Universidad de Valladolid, 47011 Valladolid, Spain*
(Received 23 March 2009; revised manuscript received 15 June 2009; published 3 September 2009)

Molecular-dynamics simulations of the free surface of liquid Sn have been performed using first-principles methods. The ionic density profile shows a stratification extending several atomic diameters into the bulk. The calculated reflectivity shows a marked maximum at a wave-vector transfer of the order of the inverse nearest-neighbor distance and whose origin is related to the surface layering. Moreover, we also find another weak broad maximum at much smaller wave-vector transfers. We analyze and discuss the origin of this anomalous feature, which is also exhibited by the experimental data.

DOI: 10.1103/PhysRevB.80.115403 PACS number(s): 61.25.Mv, 71.15.Pd

I. INTRODUCTION

In 1981 Rice and co-workers predicted,[1] from theoretical considerations and Monte Carlo simulations, that the atomic density near the free surface of a metallic liquid would change in a nonmonotonic way, showing a stratification in layers parallel to the interface. These oscillations would be expressed as a Bragg-like peak in the x-ray reflectivity curve, $R(q_z)$, at a wave vector related to the spacing between the layers. This experimental confirmation of surface layering was first observed, several years later, for the particular case of liquid Hg.[2,3] Since then, the reflectivity curves of other five elemental liquid metal surfaces have been measured, namely, Ga,[4] In,[5] K,[6] Sn,[7] and Bi,[8] all of them displaying (or suggesting, in the case of K) the expected layering peak; moreover, Sn and Bi have shown a weak wide shoulder at a lower q_z that is not present in the other systems.

It is not clear yet what is the mechanism behind the surface layering phenomenon and several hypothesis have been advanced. Rice and co-workers[9,10] have pointed to the interconnection between the ionic and electronic densities and that the rapid decay of the valence electronic density at the surface would induce a flat high-tension surface acting as a hard wall against which the atoms are packed. Other workers have suggested[11] that the undercoordinated atoms near the surface attempt to regain the favorable coordination they would have in the bulk liquid, resulting in an increased density in the outermost liquid part and causing the propagation of a density oscillation into the bulk part. More recently Chacon *et al.*[12] proposed that surface layering is a rather universal phenomenon, although in most cases it is frustrated by solidification, so it only appears in those systems whose melting temperature is very low compared with the critical temperature. This suggestion have received further backing by a recent x-ray reflectivity experiment,[13] where surface layering appears in a molecular nonmetallic liquid, which has a low melting point and a high critical point (like a liquid metal), leading to the conclusion that the presence of an electron gas is not necessary in yielding oscillating density profile (DP).

The interpretation of the reflectivity experiments relies on the use of models for the electronic DP probed by the x rays, whose parameters are varied to fit the measured $R(q_z)$. In this context the distorted crystal model[3] (DCM) has played a prominent role. It provides a DP with a near-surface layering whose strength decays smoothly into the bulk. The reflectivities of Ga, In, K and with some peculiarities also Hg could be well fitted with this model DP. Moreover, theoretical calculations of the DP through computer simulations of the corresponding interfaces also yielded DP with characteristics similar to those of the DCM.[9,10,14,15,22] The low-q_z shoulder found in Sn, and later also in Bi, could not be obtained sticking to the DCM, and the authors resorted to a modification of this model[7] in order to provide a DP consistent with $R(q_z)$. It has been found, however, that different modifications lead to very similar reflectivities;[8] in particular an extra layer can be added to the interface at a reduced distance as compared to the intelayer one, or at the same or even expanded distance if the density of the corresponding layer is conveniently increased above the bulk liquid value. This fact underlines the fundamental problem of nonuniqueness; rather different DP's can lead to very similar $R(q_z)$ (see, for instance, Fig. 2 in Ref. 8). Therefore there is a large uncertainty in the determination of the DP from experimental $R(q_z)$ data; for instance, the modification of the first inner instead of the outer layer of the DCM could also lead to a DP consistent with $R(q_z)$. There is a clear need of an alternative, more direct, calculation of the DP. A useful alternative is the use of computer simulations, which describe in detail the atomic positions yielding direct access to the DP.

In this paper we report such a study for the surface structure of liquid Sn (l-Sn), performed through density-functional theory[16] (DFT) based *ab initio* molecular-dynamics (AIMD) simulations. The underlying use of DFT provides the consistency between atomic and electronic properties, essential in regions of rapidly varying electron density as is the case in metallic surfaces. The computational burden is however large, and only small samples (a few hundred particles) can be studied for relatively short (few tens of ps) simulation times. Although orbital-free methods can alleviate the computational needs,[17–22] we have stuck here to the more accurate orbital-based technique, and in fact this is only the third study of a metallic liquid surface through this method, after liquid Si,[23] and Na,[24] for which however no experimental data exist.

II. COMPUTATIONAL METHOD

The AIMD calculations for the free surface of l-Sn were carried out in a slab geometry at a thermodynamic state characterized by $T=1000$ K and an ionic number density, $\rho_i=0.0341$ Å^{-3}. Specifically, we considered a slab of 202 atoms in a supercell with two free surfaces normal to the z axis. The dimensions of the slab were initially $L_x \times L_y \times L_z$, where $L_x=L_y=15.3$ Å; and $L_z=25.3$ Å. A further 8 Å of vacuum were added above and below the slab, i.e., along the z axis. Periodic boundary conditions are used in all three space dimensions. Although the periodic boundary conditions require that a particle moving out of the cell in the z direction reappears on the other side of the cell, we have not observed this event during the simulations. Finally, we note that during its evolution the slab can contract or expand so as to achieve the zero external pressure condition. For more details we refer the reader to Refs. 24–26.

The atomic configurations are generated under the Born-Oppenheimer approximation solving the Kohn-Sham DFT equations[16] on a plane-wave basis set for a given configuration, calculating the forces on the ions using the Hellman-Feynman theorem, and solving the corresponding Newton's equations for constant total energy, as implemented in the QUANTUM-ESPRESSO package.[27]

We have adopted the local-density approximation for the exchange-correlation energy functional, as parametrized by Perdew and Zunger.[28] The interaction between the 4 valence electrons of Sn and the ions has been described by a norm-conserving scalar-relativistic Troullier-Martins pseudopotential[29] with nonlinear core corrections, which was generated[27] from the atomic electron configuration $[\mathrm{Kr}]4d^{10}\ 5s^2\ 5p^2\ 5d^0$, pseudizing the all-electron potential to generate the local part and using cutoff radii in a.u. of $r_c(\mathrm{local})=2.5, r_c(s)=2.0147, r_c(p)=2.4917$ and $r_c(d)=3.0$.

The initial atomic positions within the slab were taken at random and the system was thermalized during 10 ps of simulation time. Wherefrom, microcanonical AIMD simulations were performed over 5000 time steps, which amounted to 30 ps of simulation time. We have used a plane-wave representation with an energy cutoff of 12 Ryd and the single Γ point was used in sampling the Brillouin zone. These 5000 configurations have been used in the evaluation of the properties. We stress that this computational scheme has recently been validated by its application to bulk l-Sn,[30] for which we obtained a very accurate description of several static, dynamic, and electronic properties at a thermodynamic state close to the triple point ($T=573$ K) and also at higher temperature ($T=1273$ K).

III. RESULTS

As an additional reliability check of the present calculations, we have computed the *bulk* pair distribution function, $g(r)$, which has been evaluated inside a 12 Å wide central section of the slab. The result is depicted in Fig. 1, showing a very good agreement with its experimental counterpart[31] at $T=1073$ K. The average number of near neighbors, within a distance r_m taken as that where $r^2 g(r)$ takes its first minimum value, is found to be 9.1, in good agreement with the experimentally suggested value of 9.6 neighbors.

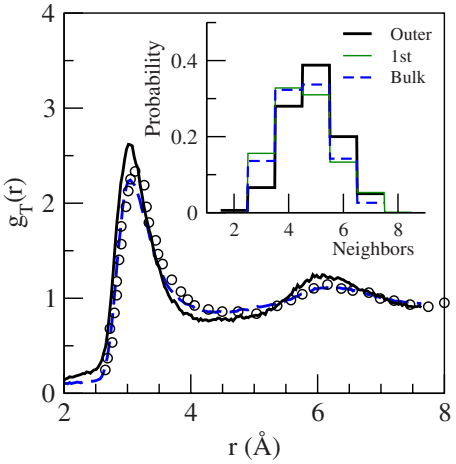

FIG. 1. (Color online) Bulk pair-correlation function (dashed blue line) and its transverse counterpart at the outer slice (full black line). The open circles stand for the bulk experimental data of Itami *et al.* (Ref. 31). The inset shows the distribution of the number of in-plane neighbors for different regions of the slab.

The longitudinal ionic DP was computed from a histogram of the particle positions relative to the slab's center of mass, so that both halves of the slab are being averaged. The obtained results are shown in Fig. 2, where we observe stratification for at least three layers into the bulk liquid. All oscillations have the same wavelength, namely $\lambda=3.1$ Å, with the outer one displaying the higher amplitude. The transverse ionic DPs, also shown in Fig. 2, are uniform as they should, with some noise substantially smaller than the amplitudes of the oscillations in the corresponding longitudinal DP. The wavelength, λ, of the ionic oscillations follows the same linear relationship with the radii of the Wigner-Seitz spheres that we have found for a wide range of simple liquid metals.[22]

The self-consistent valence electronic DP is also plotted in Fig. 2. It shows some oscillations nearly in phase with those

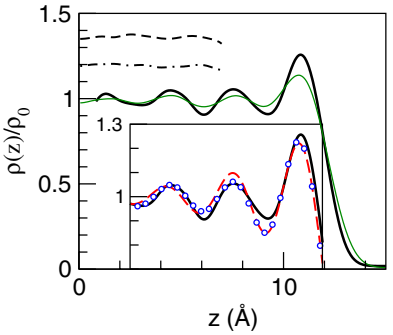

FIG. 2. (Color online) Ionic (thick black line) and valence electron (thin green line) DPs normal to the liquid-vapor interface of a liquid Sn-slab at $T=1000$ K. The densities are plotted relative to the respective bulk values. The dashed and dot-dashed lines are the x and y-transverse ionic density profiles (displaced by 0.35 and 0.2), respectively. The inset shows the ionic density profile together with its best fits to the DCM (red long-dashed line) and the sum of gaussians (blue circles).

of the ionic DP, but with an amplitude clearly smaller. In previous studies[22] covering for a wide range of simple liquid metals, we have found that all possibilities are allowed with the relative phase evolving from an opposite one, as happens for all the alkalis, to being almost in phase for Si.

Further insight into the local structure is provided by the z-dependent coordination number $n(z)$, defined as the average number of neighbors within the distance r_m. The results show that for most of the slab $n(z)$ remains practically constant ($n(z) \approx 9.1$) and close to the surface, namely, around the second outer maximum, $n(z)$ starts to decrease and reaches a value of $n(z) \approx 7.1$ at the position of the outer maximum. This $\approx 25\%$ reduction is similar to what we have already found for a wide range a simple liquid metals.[22]

Another important property concerns the structural rearrangements induced by the interface. According to Fabricius *et al.*[23] those changes may be quantified by comparison with an ideally terminated surface obtained by cutting abruptly the slab in the central region, i.e., at $z=0$. Then, $n(z)$ is evaluated at a distance z_d, which is approximately the distance between the outermost maximum and the point in the decaying tail where it takes half the bulk value. This procedure leads to a value $n(z_d)=6.5$, which is slighlty smaller than that at the outer maximum, and suggests that the surface structural rearrangement induces a small increase in the $n(z)$ over its value for an ideally terminated surface.

To analyze the slab's outer region we have partitioned the corresponding ionic DP into slices located between consecutive minima of the oscillations, with the outer slice stretching from the outermost minimum to the point in the decaying tail where it takes half its bulk value. We note that all the slices, including the outer one have the same width. However, the outer slice has a total ionic number density greater ($\approx 7\%$) than the bulk value whereas all the other inner slices have already the bulk value. This partitioning allows analyzing the in-plane order within the slices. First, we have studied the possible variations exhibited by the transverse pair-correlation functions, $g_T(r)$, across the interface. This is shown in Fig. 1 which depicts the $g_T(r)$ corresponding to the outer slice whereas that of the first inner slice already coincides with the bulk one. For the outer slice, its associated $g_T(r)$ has a main peak whose position practically coincides with that in the bulk but its height is somewhat higher; however, its first minimum and second peak are slightly shifted toward smaller r values.

For each slice, we have also calculated the distribution of the number of nearest neighbors and the results are plotted as an inset in Fig. 1. The bulk values have been obtained by using a slice of the same width as the outermost one located at the center of the slab. The results show that in the outer slice, a fraction of $\approx 40\%$ atoms have fivefold coordination although there are also significant fractions with four and six neighbors. Notice that when moving inside the slab, we obtain a reduction in the fractions of five and sixfold coordinations along with some increase in the three and fourfold coordinations. Similar results were obtained in the recent AIMD simulations[24] of the free liquid surface of Na where its outermost slice is dominated by fivefold coordinated atoms although with noticeable fractions of fourfold and sixfold coordinations.

The x-ray reflectivity experiments performed on a free liquid surface probe the total electronic density, including core and valence electrons. A first step toward a comparison with experimental data includes therefore the construction of the longitudinal total electron-density profile (TEDP) from the AIMD simulations. Another essential point to consider is the existence of thermally induced capillary waves in the surface. This leads to a roughening of the surface, and when an average over the transverse planes is performed (due to the geometry of the experiment) the profile is consequently somewhat blurred, leading to important effects in the measured reflectivity. It must be noted that capillary waves are also present in the simulations, although in smaller magnitude because of the smaller size of the simulation box, as compared to the illuminated area in the experimental sample. Taking this into account, the experimental reflectivity, $R(q_z)$, is

$$\frac{R(q_z)}{R_F(q_z)} = |\Phi_{\text{int}}(q_z)|^2 \exp(-\sigma_c^2 q_z^2), \tag{1}$$

where q_z is the momentum transfer perpendicular to the interface, $R_F(q_z)$ is the Fresnel reflectivity of a perfectly sharp step-function interface, σ_c is an effective capillary-wave roughness, and $\Phi_{\text{int}}(q_z)$ is the intrinsic surface structure factor defined as

$$\Phi_{\text{int}}(q_z) = \frac{1}{\rho_{e0}} \int_{-\infty}^{\infty} \left(\frac{\partial \rho_{e,\text{int}}(z)}{\partial z} \right) \exp(iq_z z) dz, \tag{2}$$

where ρ_{e0} is the bulk total electron density and $\rho_{e,\text{int}}(z)$ is the *intrinsic* (i.e., in the absence of capillary-wave smearing) TEDP normal to the surface. The exponential term in Eq. (1) accounts for the effect of surface roughness, and it is usually written as a sum of two contributions, $\sigma_c^2 = \sigma_0^2 + \sigma_{cw}^2$, where

$$\sigma_{cw}^2 = \frac{k_B T}{2\pi\gamma} \log\left(\frac{q_{\max}}{q_{\min}} \right), \tag{3}$$

and σ_0 represents an intrinsic surface roughness whose origin is not clear, but whose inclusion has proved essential in order to properly describe the experimental reflectivity data.[3–6,14] In Eq. (3) k_B is Boltzmann's constant, γ is the surface tension, and $q_{\max}$ and $q_{\min}$ depend on the ionic diameter and the instrumental resolution, respectively. A usual choice is $q_{\max} = \pi/a$ with a being the ionic diameter.

Figure 3 shows the experimental result for the squared modulus of the surface structure factor, $|\Phi_{\text{int}}(q_z)|^2$, corresponding to l-Sn at $T=513$ K, which was derived from the experimental x-ray reflectivity data[7,8] by using Eq. (1). Besides the Bragg-like peak at $q_z \approx 2.2$ Å^{-1}, there is also a low-angle weak wide shoulder at $q_z \approx 0.9$ Å^{-1}, which is a feature not found in any other liquid metal excepting[8] Bi. Obviously, this low-angle shoulder must be related to some other characteristic feature in the longitudinal TEDP. In order to identify this feature, a modification of the DCM was proposed. In the DCM the liquid metal is modeled by layers parallel to the surface that represent planes of atoms separated by a distance d but whose width increases as they get

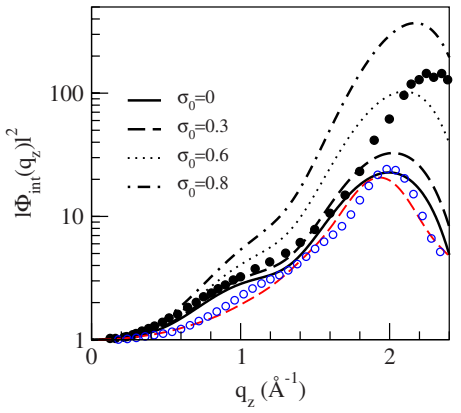

FIG. 3. (Color online) Squared modulus of the intrinsic surface structure factor of the Sn surface at $T=1000$ K, as derived from the calculated AIMD density profile (thick black lines). The full circles are the experimental data for $T=513$ K. The different dashings of the thick black lines correspond to different values of σ_0 (in Å) as shown on the graph. The thin red dashed line corresponds to the fit of the DP to the DCM, and the open blue circles are the fit to the sum of gaussians.

deeper below the surface. Mathematically, the TEDP is described by a semi-infinite sum of equally spaced Gaussians which have equal integrated areas,

$$\frac{\rho_e(z)}{\rho_{e0}} = \sum_{n=0}^{\infty} \frac{d/\sigma_n}{\sqrt{2\pi}} \exp[-(z-nd)^2/2\sigma_n^2] * F_{\mathrm{At}}(z), \qquad (4)$$

where $*$ denotes convolution, $F_{\mathrm{At}}(z)$ is the atomic scattering form factor, and

$$\sigma_n^2 = n\bar{\sigma}^2 + \sigma_0^2, \qquad (5)$$

where $\bar{\sigma}$ and σ_0 are constants. This expression for σ_n produces an increase in the Gaussian width with distance below the surface, so that the parameter $\bar{\sigma}$ is related to the decay length for surface layering. As a consequence the DCM approaches the bulk density, ρ_{e0}, for $z \gg d$. The DCM has successfully described the measured reflectivity data in l-Ga, In, K and, with some additional assumptions, in l-Hg too. However when applied to l-Sn, it had to be modified by introducing another Gaussian, of variable density and width, above the surface at a distance which may be greater, equal, or smaller than d, but whose net effect is to induce an average electron density at the surface which was greater than in the bulk.[7,8] The results of this modified DCM-type fitting performed in Ref. 8 have not rendered a clear image of the associated TEDP because although the inner oscillations have a wavelength ≈ 2.85 Å, the outer (slice) oscillation can change widely though still yielding a reasonable fitting of the experimental data. Finally, it was posited that an increase in the total electronic density above its bulk value is an essential ingredient for the appearance of the low-q_z shoulder. However, this claim does not bear well with other *ab initio* calculations[14] we have performed for l-In and l-Ga because in both systems the associated TEDP at the outer slice had an increase of 9% and 14%, respectively, and their calculated reflectivity curves did not show any special feature at low q_z.

We recall that the outer slice obtained in the present simulations shows a 7% increase in the density, but we want to find out if this is really the ultimate cause for the appearance of the low-q_z feature. We have therefore proceeded to calculate the intrinsic surface structure factor, $|\Phi_{\mathrm{int}}(q_z)|^2$, from the results of the present AIMD study. Starting from the calculated longitudinal ionic DP, we have constructed the corresponding longitudinal TEDP—namely, $\rho_e(z)$—by adding the self-consistent AIMD valence electronic DP and the total core electronic DP obtained by superposing at the ionic sites the core electronic density found in the pseudopotential construction.[14,15,18,19,24] The core densities are rather narrow and their superposition gives a profile in complete phase with the ionic DP. Moreover, the Sn atom has 46 core electrons and four valence electrons, which implies that the addition of the total core and valence electronic densities leads to a total $\rho_e(z)$, whose shape, after normalization with respect to its bulk value, practically coincides with the ionic DP already depicted in Fig. 2.

Still we have to take into account the fact that the $\rho_e(z)$ obtained this way is not the intrinsic one because it includes some capillary waves as corresponds to the temperature and the dimensions of the simulation box. These fluctuations can be reasonably described in terms of an associated $\sigma_{cw}^{\mathrm{AIMD}}$ defined in Eq. (3). Therefore, a comparison with the experimental data will previously require properly accounting for these effects; this is done as follows. From the calculated $\rho_e(z)$, we obtain the following expression for its associated reflected intensity:

$$\left[\frac{R(q_z)}{R_F(q_z)}\right]\exp(\sigma_0^2 q_z^2) = |\Phi(q_z)|^2 = \left|\frac{1}{\rho_{e0}}\int_{-\infty}^{\infty}\left(\frac{\partial\rho_e(z)}{\partial z}\right)\exp(iq_z z)dz\right|^2. \qquad (6)$$

Comparison with Eq. (1) shows that the AIMD calculated surface structure factor $\Phi(q_z)$ may be envisaged as the result of a convolution of the intrinsic one, $\Phi_{\mathrm{int}}(q_z)$, with an associated Gaussian distribution describing the thermal fluctuations in the simulation quantified by $\sigma_{cw}^{\mathrm{AIMD}}$. For its evaluation we have used the values[32] $\gamma=515$ mN/m, $a=3.0$ Å, and $L=15.3$ Å, which leads to $\sigma_{cw}^{\mathrm{AIMD}}=0.83$ Å. As for the intrinsic surface roughness σ_0, and because of its non well-defined status, we have chosen to perform calculations using different values within the range $0 \le \sigma_0 \le 1$. The results are shown in Fig. 3 where we have depicted the corresponding results for $|\Phi_{\mathrm{int}}(q_z)|^2$. All curves have a main peak located at $q_z \approx 2.0$ Å^{-1}, which is a consequence of the surface layering with a wavelength ≈ 3.1 Å. Notice that the main maximum is located at a smaller q_z than in the experiment because the present AIMD calculations correspond to a higher temperature state. But the most striking feature is the appearance, in all the calculated curves, of a shoulder at around $q_z \approx 1.0$ Å^{-1}. This feature qualitatively agrees with the similar shoulder in the experimental data for l-Sn at $T=513$ K (also shown in Fig. 3) and it is sensible to assume that they must share a common origin.

To investigate the origin of the low-q_z shoulder we have made several modifications to the AIMD TEDP in order to find out which of its features has the strongest influence on the position and/or magnitude of the shoulder. In all the following calculations we have assumed, for simplicity, that $\sigma_0=0$. First we have checked the claim[8] that the shoulder is related to an increased total electronic density in the outer layer. To this end, we have again calculated the $|\Phi_{\text{int}}(q_z)|^2$ associated to TEDPs, in which the shape of the outer slice has been modified so as to change its associated total electronic density by a factor within the range 0.6–1.6. In all cases the position and magnitude of the low-q_z shoulder in $|\Phi_{\text{int}}(q_z)|^2$ remained virtually unchanged. We have also analyzed whether the shoulder would be related to the decaying tail in the TEDP, namely to its shape from the outer maximum outwards. The $|\Phi_{\text{int}}(q_z)|^2$ was calculated using TEDPs, in which the slope of the decaying tail was multiplied by a factor within the range 0.6–1.4. Again, the shoulder still appeared although its position moved to slightly smaller (greater) q_z values when the factor was greater (smaller) than unity. Consequently, it seems reasonable to conclude that the existence of the low-q_z shoulder has no direct relation (if any) with the magnitude and shape of the outer slice in our TEDP.

Going back to Fig. 2 we note that the AIMD calculated ionic (and total electronic) DP for l-Sn has the atypical characteristic that the oscillations in the first and second inner slices have virtually the same amplitude. This is a feature not found in any of our previous AIMD simulations for other liquid metals.[14,22] In those simulations we found that the amplitude of the oscillation in the outer slice could be greater or smaller than that in the first inner slice but the oscillation in the second inner slice had always a smaller amplitude than the previous one. To analyze the influence of this feature on the reflectivity, we have again calculated the $|\Phi_{\text{int}}(q_z)|^2$ corresponding to a TEDP in which the amplitude of only the first inner oscillation was smoothly increased by a factor in the range 1.0–1.6. The results are plotted in Fig. 4 which shows both the modified TEDPs and the associated reflectivities. Notice that as the amplitude of the first inner oscillation is increased, the low-q_z shoulder became weaker and completely disappears when the amplitude is increased by a factor ≈ 1.5. Furthermore, a similar calculation performed using a TEDP in which the amplitude of only the second inner slice was decreased by a factor within the range 1.0–0.6 produced a similar effect, namely, the low-q_z shoulder became weaker and it completely disappeared when the amplitude was diminished by a factor 0.6.

Finally, a calculation using a TEDP in which the amplitudes of the first and second inner slices is simultaneously increased and decreased respectively leads to a total disappearance of the low-q_z shoulder when the first inner oscillation is increased by a factor 1.2 and that of the second inner slice was decreased by a factor 0.8. This is depicted in Fig. 5, which shows both the modified TEDPs along with the respective reflectivities. We recall that in all the above calculations, the shape of $|\Phi_{\text{int}}(q_z)|^2$ remained practically unaltered for $q_z \geq 1.6$ Å^{-1}.

In conclusion, it appears that the ultimate reason for the existence of the low-q_z shoulder is related to the peculiar

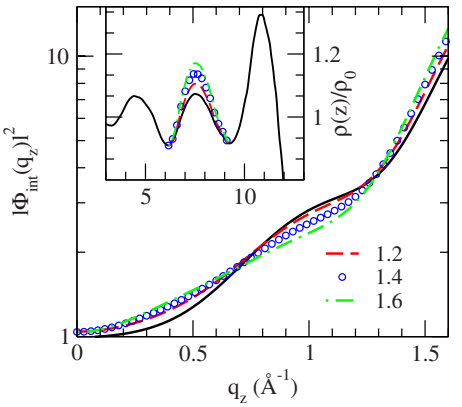

FIG. 4. (Color online) Squared modulus of the intrinsic surface structure factor of the Sn surface at $T=1000$ K, in the region of the shoulder around $q_z \approx 1$ Å^{-1}. The thick black curve is the result from the AIMD TEDP. The red dashed, open blue circles and dashed dotted lines are the results obtained by enhancing the first inner oscillation by a factor of 1.2, 1.4 and 1.6 respectively. The inset shows the corresponding (normalized) TEDPs.

behavior of the TEDP in the region comprising the first and second inner slices. Indeed, the incapability of the DCM to produce a low-q_z shoulder is also consistent with the behavior of the TEDP in this region We have tried to fit our calculated TEDP by using the DCM, and the best fit was achieved with the following values: $d=3.14$ Å, $\bar{\sigma}^2=0.43$ Å^2, and $\sigma_0^2=1.13$ Å^2. This is plotted in the inset of Fig. 2, where we notice that the DCM can reproduce rather well the outer slice but is completely unable to provide a reasonable description of the first inner layer whose amplitude is enhanced. The associated $|\Phi_{\text{int}}(q_z)|^2$ is depicted in Fig. 3 where it is observed a fair agreement with the AIMD one except for the total absence of the low-q_z shoulder. Some improvement can be achieved if the fitting is performed with a modified DCM in which the condition given by Eq. (5) is removed, so that the σ_n are now used as fitting parameters.

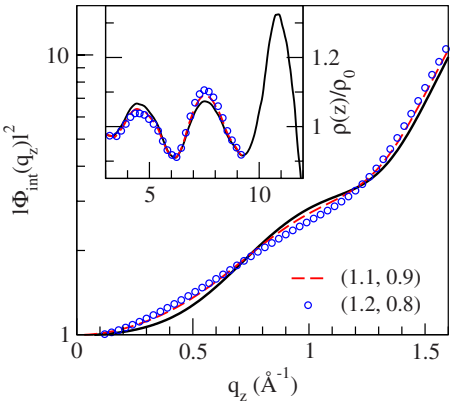

FIG. 5. (Color online) Squared modulus of the intrinsic surface structure factor of the Sn surface at $T=1000$ K, in the region of the shoulder around $q_z \approx 1$ Å^{-1}. The thick black curve is the result from the AIMD TEDP. The red dashed line (open blue circles) is the result of simultaneously varying the amplitudes of the first and second inner by factors 1.1 (1.2) and 0.9 (0.8), respectively. The inset shows the corresponding (normalized) TEDPs.

This leads to values $d=3.10$ Å, $\sigma_0^2=1.09$, $\sigma_1^2=1.57$, $\sigma_2^2=1.81$, $\sigma_3^2=2.09$, and $\sigma_4^2=2.29$ (all of them in Å^2). This procedure renders a much improved description of the AIMD TEDP although there still remain some discrepancies which are located at the region of the minimum between the outermost and the first inner slice, which is somewhat overestimated. Moreover, the corresponding $|\Phi_{\text{int}}(q_z)|^2$, also plotted in Fig. 3, shows a weak shoulder located at a $q_z \approx 1.2$ Å^{-1}.

IV. CONCLUSIONS

We have presented results of *ab initio* simulations for the free liquid surface of l-Sn. It exhibits surface layering, which is a feature already found in other liquid metals. Besides the usual layering peak, the AIMD calculated intrinsic surface structure factor displays an additional low-q_z shoulder at ≈ 1.0 Å^{-1}, which exactly coincides with a similar feature already found in the experimental reflectivity data. Although the origin of this feature was originally ascribed to an outermost layer at a distance reduced by 10% relative to the subsequent ones,[7] or to an increased density in the outermost layer,[8] our AIMD results do not support these ideas. Such a model certainly produces the shoulder, but it is not the only one that does so. Our profile also leads to a feature at the correct q_z and is derived from first principles. In fact, the calculated ionic DP shows layers whose distance remains constant and the reason for the appearance of this shoulder has been found to lie in the peculiar behavior of the TEDP in the region comprising the first and second inner slices.

ACKNOWLEDGMENTS

L.C. acknowledges the financial support of the Ministerio de Educacion y Ciencia of Spain (Grant No. SB2005-0062). L.E.G. and D.J.G. acknowledge the support of the MCINN (Grant No. FIS2008-02490/FIS), the EU FEDER program, and JCyL (Grant No. GR120).

[1] M. P. D'Evelyn and S. A. Rice, Phys. Rev. Lett. **47**, 1844 (1981).
[2] S. W. Barton, B. N. Thomas, F. Novak, P. M. Weber, J. Harris, P. Dolmer, J. M. Bloch, and S. A. Rice, Nature (London) **321**, 685 (1986).
[3] O. M. Magnussen, B. M. Ocko, M. J. Regan, K. Penanen, P. S. Pershan, and M. Deutsch, Phys. Rev. Lett. **74**, 4444 (1995); E. DiMasi, H. Tostmann, B. M. Ocko, P. S. Pershan, and M. Deutsch, Phys. Rev. B **58**, R13419 (1998).
[4] M. J. Regan, E. H. Kawamoto, S. Lee, P. S. Pershan, N. Maskil, M. Deutsch, O. M. Magnussen, B. M. Ocko, and L. E. Berman, Phys. Rev. Lett. **75**, 2498 (1995).
[5] H. Tostmann, E. DiMasi, P. S. Pershan, B. M. Ocko, O. G. Shpyrko, and M. Deutsch, Phys. Rev. B **59**, 783 (1999).
[6] O. G. Shpyrko, P. Huber, A. Y. Grigoriev, P. S. Pershan, B. Ocko, H. Tostmann, and M. Deutsch, Phys. Rev. B **67**, 115405 (2003).
[7] O. G. Shpyrko, A. Y. Grigoriev, C. Steimer, P. S. Pershan, B. Lin, M. Meron, T. Graber, J. Gerbhardt, B. Ocko, and M. Deutsch, Phys. Rev. B **70**, 224206 (2004).
[8] P. S. Pershan, S. E. Stoltz, O. G. Shpyrko, M. Deutsch, V. S. K. Balagurusamy, M. Meron, B. Lin, and R. Streitel, Phys. Rev. B **79**, 115417 (2009).
[9] M. Zhao, D. S. Chekmarev, Z.-H. Cai, and S. A. Rice, Phys. Rev. E **56**, 7033 (1997).
[10] D. Chekmarev, M. Zhao, and S. A. Rice, J. Chem. Phys. **109**, 768 (1998).
[11] S. Iarlori, P. Carnevali, F. Ercolessi, and E. Tosatti, Surf. Sci. **211-212**, 55 (1989).
[12] E. Chacón, M. Reinaldo-Falagan, E. Velasco, and P. Tarazona, Phys. Rev. Lett. **87**, 166101 (2001); E. Velasco, P. Tarazona, M. Reinaldo-Falagan, and E. Chacón, J. Chem. Phys. **117**, 10777 (2002).
[13] H. Mo, G. Evmenenko, S. Kewalramani, K. Kim, S. N. Ehrlich, and P. Dutta, Phys. Rev. Lett. **96**, 096107 (2006).
[14] D. J. González and L. E. González, J. Phys.: Condens. Matter **20**, 114118 (2008).
[15] L. E. González and D. J. González, Phys. Rev. B **77**, 064202 (2008).
[16] P. Hohenberg and W. Kohn, Phys. Rev. **136**, B864 (1964); W. Kohn and L. J. Sham, *ibid.* **140**, A1133 (1965).
[17] F. Perrot, J. Phys.: Condens. Matter **6**, 431 (1994); E. Smargiassi and P. A. Madden, Phys. Rev. B **49**, 5220 (1994); M. Foley and P. A. Madden, *ibid.* **53**, 10589 (1996).
[18] D. J. González, L. E. González, J. M. López, and M. J. Stott, J. Chem. Phys. **115**, 2373 (2001); Phys. Rev. B **65**, 184201 (2002).
[19] L. E. González, D. J. González, and J. M. López, J. Phys.: Condens. Matter **13**, 7801 (2001).
[20] D. J. González, L. E. González, and M. J. Stott, Phys. Rev. Lett. **92**, 085501 (2004).
[21] D. J. González, L. E. González, and M. J. Stott, Phys. Rev. Lett. **94**, 077801 (2005); J. Blanco, D. J. González, L. E. González, J. M. López, and M. J. Stott, Phys. Rev. E **67**, 041204 (2003); D. J. González, L. E. González, J. M. López, and M. J. Stott, *ibid.* **69**, 031205 (2004).
[22] L. E. González, D. J. González, and M. J. Stott, J. Chem. Phys. **123**, 201101 (2005); D. J. González, L. E. González, and M. J. Stott, Phys. Rev. B **74**, 014207 (2006).
[23] G. Fabricius, E. Artacho, D. Sanchez-Portal, P. Ordejon, D. A. Drabold, and J. M. Soler, Phys. Rev. B **60**, R16283 (1999).
[24] B. G. Walker, C. Molteni, and N. Marzari, J. Phys.: Condens. Matter **16**, S2575 (2004); J. Chem. Phys. **124**, 174702 (2006); **127**, 134703 (2007).
[25] E. Salomons and M. Mareschal, J. Phys.: Condens. Matter **3**, 3645 (1991).
[26] S. W. Sides, G. S. Grest, and Martin-D. Lacasse, Phys. Rev. E **60**, 6708 (1999).
[27] S. Baroni, A. Dal Corso, S. de Gironcoli, P. Giannozzi, C. Cavazzoni, G. Ballabio, S. Scandolo, G. Chiarotti, P. Focher, A. Pasquarello, K. Laasonen, A. Trave, R. Car, N. Marzari, and A. Kokalj, http://www.pwscf.org/.

[28] D. M. Ceperley and B. J. Alder, Phys. Rev. Lett. **45**, 566 (1980); J. P. Perdew and A. Zunger, Phys. Rev. B **23**, 5048 (1981).
[29] N. Troullier and J. L. Martins, Phys. Rev. B **43**, 1993 (1991).
[30] L. Calderin, D. J. Gonzalez, L. E. Gonzalez, and J. M. Lopez, J. Chem. Phys. **129**, 194506 (2008).
[31] T. Itami, S. Munejiri, T. Masaki, H. Aoki, Y. Ishii, T. Kamiyama, Y. Senda, F. Shimojo, and K. Hoshino, Phys. Rev. B **67**, 064201 (2003).
[32] T. Iida and R. I. L. Guthrie, *The Physical Properties of Liquid Metals* (Clarendon, Oxford, 1988).